EFFECT OF BEARING PADS ON PRECAST PRESTRESSED CONCRETE BRIDGES

By Nur Yazdani,[1] P.E., Fellow, ASCE, Scott Eddy,[2] Member, ASCE, and Chun S. Cai,[3] P.E.

ABSTRACT: Precast AASHTO concrete bridge I-beams are often supported at the ends by elastomeric bearing pads. The bearing pad-bridge beam interface defines support boundary conditions that may affect the performance of the bridge. In this study, finite-element modeling was used to validate AASHTO bearing stiffness specifications. Stiffness characteristics of the Florida DOT bearing pads were theoretically determined under varying elastomer shear modulus values. Finite-element models of AASHTO Types III and V beams were subjected to simulated static truckloads. Vertical and horizontal spring elements simulating new bearing pads were incorporated at the ends of the beam models. A full section of a bridge on U.S. Route 27 was also modeled, and the results were compared with field tests. In general, the restraint effects of the bearing pads are beneficial to the performance of the beams and the bridge. The beneficial effect, however, is small for new bearing pads and more pronounced under a drastic increase in bearing stiffness due to aging and colder temperatures. Such a dramatic increase in bearing stiffness must be justified if the beneficial elements are to be utilized. Current Florida DOT bearing pads are serving the main purpose of their application, which is to provide minimum horizontal restraint force to the beams while allowing horizontal movement.

INTRODUCTION

Precast prestressed concrete bridge I-beams are widely used in many states, including Florida. These beams are often supported by elastomeric bearing pads. The Florida DOT (FDOT) currently specifies that all pads supporting AASHTO precast concrete I-beams should utilize steel-laminated neoprene pads (''Structures'' 1997). Pictures of a bearing pad supported beam and various bearing pads are shown in Fig. 1.

Elastomeric bearing pads are designed to support the vertical compressive loads from bridge beams and to allow horizontal movement of beams due to thermal expansion and contraction, traffic loads, elastic shortening, beam end rotations, and time-dependent changes in concrete. This is accomplished by utilizing alternating layers of steel and neoprene, which allows horizontal movement of the top and bottom bearing surfaces relative to one another. Under service loads, the elastomer deflects vertically and horizontally and provides a limited amount of vibration damping to the bridge superstructure. When properly designed, the elastomer has the ability to return to its original shape without experiencing excessive permanent deformation under normal service loads. Elastomeric bearings have desirable performance characteristics including simplicity, maintenance-free durability, and economy.

Conditions at the bearing pad-beam interface define boundary conditions that may affect the performance of the bridge superstructure. Design standards have been developed to provide guidelines for the proper selection of the bearing pads. However, questions exist about the performance of concrete bridge I-beams as a result of the support boundary conditions created by the elastomeric bearing pads. The bearing pads are designed with certain simplifying assumptions such as material and geometric linearity (AASHTO 1996a). Precast I-beams are designed with simplifying assumptions such as simple support conditions and an overall transmission of 5% of the live load from the superstructure to the substructure (AASHTO 1996a). AASHTO also states that the forces imposed by the bearing on the substructure are a function of the stiffness of the bearing and the flexibility of the substructure and that such forces shall be incorporated into the design of substructure components. However, AASHTO does not address incorporation of these forces into the design of the beams. It is possible that bridges are stronger in actual service as a result of restraining forces at the bearing pad-beam interface.

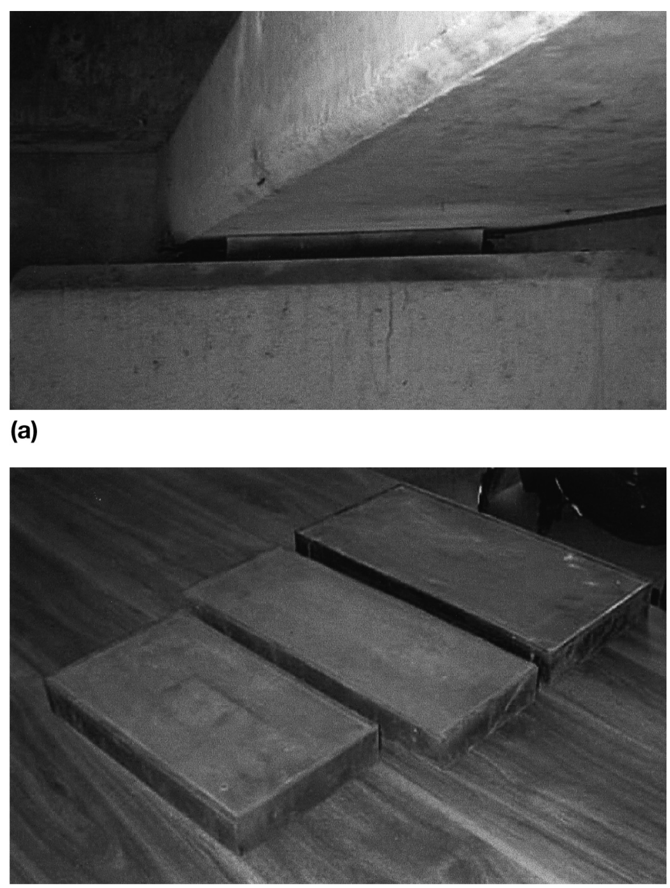

(a)

(b)

FIG. 1. Bearing Supported Beam and Bearing Pads: (a) Bearing Pad Supported Beam End; (b) Individual FDOT Bearing Pads

[1]Prof. of Civ. Engrg., Florida A. & M. Univ.—Florida State Univ. College of Engrg., 2525 Pottsdamer St., Tallahassee, FL 32310.

[2]Proj. Engr., The Coloney Company Consulting Engineers, Inc., 1014 N. Adams St., Tallahassee, FL 32303.

[3]Sr. Struct. Engr., Struct. Res. Ctr., Florida Dept. of Transp., 2007 E. Paul Dirac Dr., Tallahassee, FL 32310.

Note. Discussion open until January 1, 2001. To extend the closing date one month, a written request must be filed with the ASCE Manager of Journals. The manuscript for this paper was submitted for review and possible publication on February 5, 1999. This paper is part of the ***Journal of Bridge Engineering***, Vol. 5, No. 3, August, 2000. ©ASCE, ISSN 1084-0702/00/0003-0224–0232/$8.00 + $.50 per page. Paper No. 20202.

PREVIOUS RESEARCH

Researchers with the Ontario Ministry of Transportation and Communication tested a slab-on-beam bridge, built in 1973, to determine why the bridge appeared stiffer in flexure than predictions from analysis (Bakht 1988a). This bridge consists of five steel plate girders with a composite concrete deck slab. Tests revealed that the restraint from elastomeric bearing supports resulted in the reduction of the girder live load moment by at least 9%. Dynamic testing of this bridge showed that the longitudinal flexural rigidity of the bridge was much larger than could be analytically rationalized (Billing 1984). Twenty-six other bridges in Canada were tested, leading to the conclusion that the bridges are typically stiffer than design assumptions. In 1985, an old slab-on-girder bridge constructed in 1953 with a span of 16.3 m was load tested (Bakht 1988b), consisting of steel bearing plates, a noncomposite concrete deck slab, and seven simply supported steel plate girders. The steel bearing plates were moderately corroded, and girder ends were pressing against the abutment wall. The restraint forces helped reduce the live load moments in the girders by a minimum of 15%.

Tests conducted on bridges on Ontario for over 15 years showed that slab-on-girder bridges are usually stiffer in flexure than that predicted by analysis (Bakht and Jaeger 1988). A single-span steel I-girder bridge was analyzed using a 2D finite-element (FE) analysis. Single elastic springs were used to model horizontal bearing restraint, and rigid roller supports were used for the vertical reactions. This restraint resulted in a midspan deflection and bottom flange stress reduction of 12 and 18%, respectively. An ultimate load test of a 40-year-old bridge in the city of London, Ontario, Canada, was conducted (Bakht and Jaeger 1992). This bridge was made of six steel girders with a concrete deck slab, with the girders resting directly on concrete abutments. Calculations of the restraint forces indicated that the applied moments were reduced by >11%.

Pentas et al. (1995) performed a comprehensive experimental investigation to obtain thermally induced movements of a newly constructed bridge in central Louisiana. The bridge was constructed of cast-in-place concrete slabs acting compositely with segments containing Type IV AASHTO prestressed beams and other segments using steel plate girders. The bridge experienced movements at the bents due to temperature effects and thermal forces generated in the beams.

Sen and Spillet (1994) constructed a simply supported scale bridge consisting of steel beams acting compositely with a concrete slab. The maximum restraint effects occurred at the lowest temperatures with a reduction in the service moment of about 15%. It was also reported that compressive forces were present under the bottom flange near the supports (Ramachandran 1994). The test results corroborated the data obtained from other field experiments (Bakht 1988a,b).

Full-scale static and dynamic tests of two prestressed concrete bridges were performed by the FDOT to determine the actual strength of the bridges (Issa 1992). Static testing of the Interstate 75 (I-75) bridge over the Caloosahatchee River and the U.S. 27 bridge over the Suwannee River at Fanning Springs, Fla., was performed with FDOT test trucks. Conclusions were made that the two bridges possessed greater residual strength than predicted by analytical calculations, assuming simple beam supports.

It is apparent that no experimental or analytical study has been undertaken to evaluate the effect of elastomeric bearing pads on the performance of precast prestressed concrete bridge beams. Previous studies have mainly focused on field load testing of steel beam bridges. The study reported herein focused on the presence, extent, and effect of bearing pad restraint on precast prestressed bridge beams.

SPECIFICATIONS FOR ELASTOMERIC BEARING PADS

AASHTO suggests that shear modulus is the most important material property for bearing pad design and is the preferred method for specifying the elastomer (AASHTO 1996a). Engineers typically specify bearing pads according to the hardness of the elastomer because the test for hardness is quick and simple. However, results from a hardness test are variable and correlate only loosely with shear modulus. AASHTO provides a range of shear modulus values that correspond to different hardness levels. AASHTO specifies that at 23°C the elastomer used in bearing pads shall have a shear modulus of 0.655–1.379 MPa and a nominal hardness grade between 50 and 60 on the Shore A scale (AASHTO 1996a). FDOT specifies that the elastomer in all bearing pads shall have a grade 50-durometer hardness with a shear modulus range of 0.655–0.896 MPa (''Standard'' 1996). It has been shown that an increase in hardness and shear modulus occurs with a decrease in temperature (Minor and Egen 1970; Roeder et al. 1987).

The shear modulus and the shape factor control the compressive stress-strain characteristic of an elastomer. For rectangular bearings, the shape factor for one elastomer layer is given by (AASHTO 1996a)

$$S = \frac{LW}{2h_{ri}(L + W)} \tag{1}$$

where S = shape factor from a layer of an elastomeric bearing; L = dimension of bearing parallel to longitudinal beam axis; W = dimension of bearing normal to beam axis; and h_{ri} = thickness of a single elastomer layer. Table 1 lists elastomeric bearing pads specified by the FDOT together with design parameters, bearing pad dimensions, and properties. The shape factor for each layer was calculated by (1). The overall shape factor for the bearing pad was calculated using the weighted average of the individual elastomer layer thicknesses and shape factors.

It is difficult to quantify the restraint stiffness in actual bridges. Design specifications provide simplified expressions for stiffness of new bearings. The effective compressive modulus of elasticity, taking into account the restraint of bulging, is given by

$$E_c = 3G(1 + kS^2) \quad \text{(AASHTO 1996a)} \tag{2}$$

$$E_c = 6GS^2 \quad \text{(AASHTO 1996b)} \tag{3}$$

where E_c = effective compressive modulus; G = shear modulus of the elastomer; and k = empirical constant dependent on elastomer hardness = 0.75 for 50-durometer neoprene.

TABLE 1. Physical Parameters for FDOT Bearing Pads (“Structures” 1997)

Parameter (1)	II/II (2)	III/III (3)	IV/IV (4)	V/V, VI, and Florida bulb tee (5)
Length (mm)	204	178	230	254
Width (mm)	356	458	458	610
Area (mm^2)	72,625	81,524	105,350	154,940
Elastomer thickness (mm)				
Inner layers (2)	8.75	7.75	10.75	12.75
Outer layers (2)	6.00	6.00	6.00	6.00
Total	29.50	27.50	33.50	37.50
Shape factor				
Inner layers	7.4	8.3	7.1	7.0
Outer layers	10.8	10.7	12.8	14.9
Weighted shape factor for pad	8.8	9.3	9.1	9.6

VALIDATION OF AASHTO MODULI

Equivalent bearing stiffnesses were calculated herein for FDOT bearing pads based on FE modeling using an eight-node cubic linear element from ANSYS 5.4 software (ANSYS 1995). The calculated stiffnesses were compared with AASHTO predicted values. As shown in Fig. 2, typical bearing pads were assumed to be restrained by rigid top and bottom plates. The behavior of neoprene and steel reinforcement were assumed to be elastic. Vertical, horizontal, and moment forces were applied to the model in sequence to predict bearing stiffnesses. Six values of stiffness were derived based on beam theory as follows:

$$k_x = \frac{EA_x}{H} = \frac{P_x}{\Delta_x} \tag{4}$$

$$k_y = \frac{GA_y}{H} = \frac{P_y}{\Delta_y - \dfrac{P_y H^3}{3EI_y}} = \frac{P_y}{\Delta_y - \dfrac{P_y H^2}{3k_{Ry}}} \tag{5}$$

$$k_z = \frac{GA_z}{H} = \frac{P_z}{\Delta_z - \dfrac{P_z H^3}{3EI_z}} = \frac{P_z}{\Delta_z - \dfrac{P_z H^2}{3k_{Rz}}} \tag{6}$$

$$k_{Rx} = \frac{GI_x}{H} = \frac{M_x}{\Delta_{Rx}} \tag{7}$$

$$k_{Ry} = \frac{EI_y}{H} = \frac{M_y}{\Delta_{Ry}} \tag{8}$$

$$k_{Rz} = \frac{EI_z}{H} = \frac{M_z}{\Delta_{Rz}} \tag{9}$$

where P_x, P_y, P_z, M_x, M_y, and M_z = forces and moments applied in x-, y-, and z-directions, respectively; Δ_x, Δ_y, Δ_z, Δ_{Rx}, Δ_{Ry}, and Δ_{Rz} = deflections and rotations corresponding to P_x, P_y, P_z, M_x, M_y, and M_z, respectively; k_x, k_y, k_z, k_{Rx}, k_{Ry}, and k_{Rx} = equivalent stiffness corresponding to Δ_x, Δ_y, Δ_z, Δ_{Rx}, Δ_{Ry}, and Δ_{Rz}, respectively; E = modulus of elasticity; and A_x, A_y, A_z, I_x, I_y, and I_z = areas and moments of inertia corresponding to each axis; and H = total thickness of the bearing excluding the rigid plates.

The predicted stiffnesses are presented in Table 2. Material properties used in the modeling are as follows: for neoprene, Poisson's ratio = 0.4985, E = 2.28 MPa, and G = 0.76 MPa and for steel, Poisson's ratio = 0.3, E = 199,938 MPa, and G = 79,285 MPa. Element layers of 9, 24, and 12 were used in the x-, y-, and z-directions, respectively. An alternate 9, 36, and 15 layering was used for the FDOT Type V bearing pad, with negligible differences in results compared to the coarser mesh.

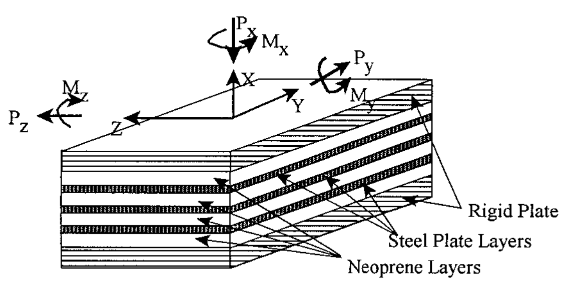

FIG. 2. Forces and Moments for FE Analysis of Bearing Pads

TABLE 2. Stiffness of FDOT Bearing Pads Based on FE Modeling

Stiffness (kN/mm) (1)	FDOT Bearing Type II (2)	III (3)	IV (4)	V (5)	II* (6)	II*/II (7)
k_x	622	748	792	1,042	25,379	40.78
k_y	1.87	2.25	2.39	3.09	93.51	49.98
k_z	1.87	2.25	2.39	3.09	93.42	49.97
k_{Rx}	40.7	70.2	81.0	177	2,033	49.97
k_{Ry}	2.16×10^6	1.98×10^6	3.50×10^6	5.60×10^6	8.77×10^7	40.65
k_{Rz}	6.58×10^6	1.31×10^7	1.39×10^7	3.24×10^7	2.77×10^8	42.05

Note: For type II*, shear modulus G^* = 50G.

TABLE 3. Stiffnesses of FDOT Bearing Pads [Based on AASHTO (1996) Standard Specifications]

Stiffness and other parameters (1)	Bearing Type II (2)	III (3)	IV (4)	V (5)
I_y (mm^4)	2.52×10^8	2.15×10^8	4.64×10^8	8.33×10^8
G (MPa)	0.76	0.76	0.76	0.76
E_c (MPa)	267	297	285	317
k_x (kN/mm)	656	882	896	1,309
k_z (kN/mm)	1.87	2.25	2.38	3.13
k_{Ry} (kN/mm)	2.28×10^6	2.33×10^6	3.95×10^6	7.04×10^6

Elastomers may experience significant stiffening due to aging and cold temperatures. The increase in stiffness may be as high as 50 times the original stiffness (Roeder et al. 1989). The neoprene shear modulus was increased 50 times over the new pad shear modulus for the FDOT Type II bearing pad model, designated as II* in Table 2. As shown in the table, the shear stiffnesses k_y and k_z and torsional stiffness k_{Rx} increase about 50 times, whereas the vertical stiffness k_x and bending stiffnesses k_{Ry} and k_{Rz} increase about 41 times from the Type II model to the Type II* model. Therefore, it may be inferred that the shear stiffness of the bearing pads have a linear relationship to the shear modulus of neoprene and that the vertical and bending stiffnesses do not.

Calculated pad stiffnesses based on standard design specifications (AASHTO 1996a) are summarized in Table 3. Eq. (2) was used to calculate values of the effective modulus E_c. The AASHTO provisions allow the determination of only the three stiffnesses shown in Table 3. It can be seen that the shear stiffness is almost identical to that from the FE analysis (Table 2). The vertical and bending stiffnesses based on the AASHTO specifications are higher than the FE predictions. This is due to the nonlinear behavior of neoprene materials considered in the development of the AASHTO formulas. It is noted that only half of the bending stiffness is used in the calculation of restraint moment in the AASHTO specifications (AASHTO 1996b, equation 14.6.3.2.2). In consideration of this reduction, the actual bending stiffness used in AASHTO is less than the FE prediction. Considering the rather large variation of neoprene materials, it may be inferred that the AASHTO specifications are applicable in the stiffness calculation, and were subsequently used in this study.

The compressive and the shear stiffnesses k_x and k_z were used to model the effect of bearing pads on AASHTO beams. The effect of the other shear stiffness k_y is expected to be negligible, because the main translation of the bearing pad in the z-direction is normal to the y-axis. The torsional stiffness k_{Rx} and the two bending stiffnesses k_{Ry} and k_{Rz} were indirectly accounted for through the modified bearing pad model, as discussed later in this paper.

OVERVIEW OF BRIDGE ANALYSIS

The variation in material properties of the elastomer due to manufacturer compounding, fillers, age, and temperature causes changes in the beam boundary conditions provided by the bearing pads. For the beam and bridge models, the shear modulus was assumed to be in the 0.68–1.43 MPa range for individual beams, corresponding to Shore A hardness grade

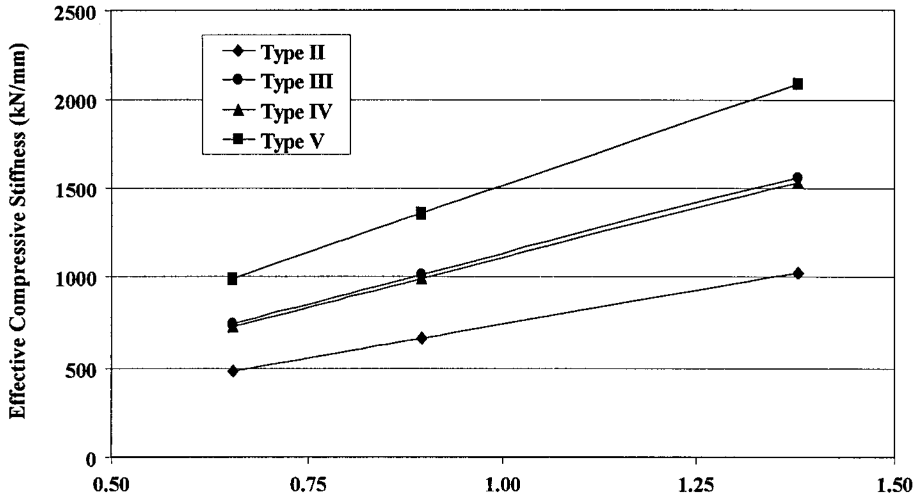

FIG. 3. Effective Compressive Stiffness for FDOT Bearing Pads

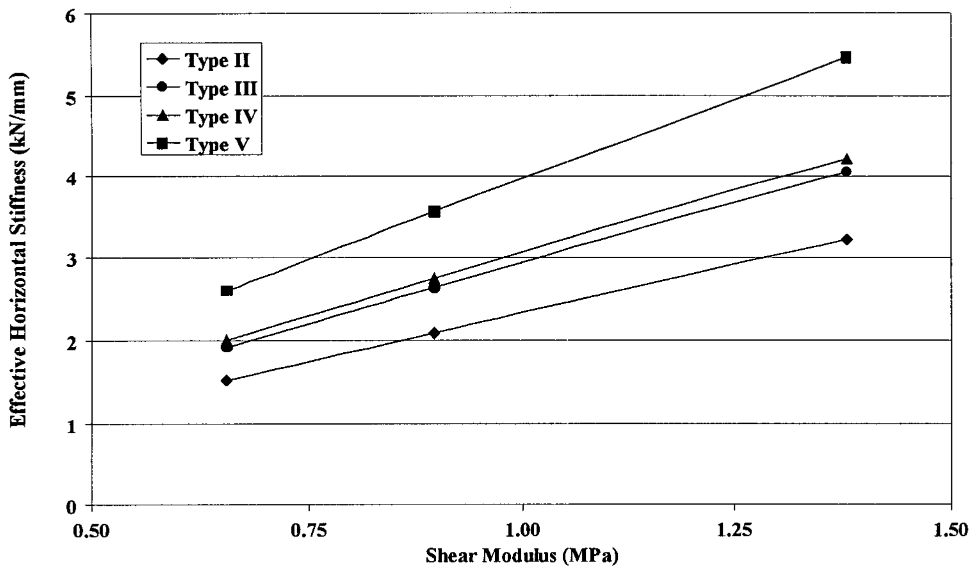

FIG. 4. Effective Horizontal Stiffness for FDOT Bearing Pads

between 50 and 60 (AASHTO 1996a). Increased shear modulus values due to aging and cold temperatures were employed for a full bridge model, as described later. Figs. 3 and 4 present the compressive and horizontal stiffnesses for the FDOT bearing pads for various shear modulus values, based on (4) and (6), respectively, which were used in the FE modeling of bridge beams.

Segments of two bridges in Florida with AASHTO concrete I-beams supported by FDOT bearing pads were selected for this study. One was the approach segments of the U.S. Route 27 bridge at Fanning Springs (hereafter called the U.S. 27 bridge). This bridge utilized 20.1-m-long AASHTO Type III beams supported by FDOT Type III bearing pads. The second bridge chosen was on I-75 in Broward County (hereafter called the I-75 bridge), which utilized 39.6-m-long AASHTO Type V beams supported by FDOT Type V bearing pads. The U.S. 27 and I-75 bridges were built in 1968 and 1996, respectively. A 35.5-MPa concrete compressive strength for the beams and 22–12.7-mm-diameter stress relieved strands with six harped tendons were specified for the U.S. 27 bridge. The beams were assumed to act compositely with the cast-in-place slab for which the concrete compressive strength was 24.1 MPa. The beams from the I-75 bridge were designed with 44.8-MPa concrete and 64–12.7-mm-diameter low relaxation prestressing strands. The strand pattern consists of 48 fully bonded strands and two sets of eight strands debonded 7.6 and 9.1 m from the ends, respectively. The composite cast-in-place slab was designed with 27.6-MPa compressive strength concrete. The cross sections of the selected bridge segments are shown in Fig. 5.

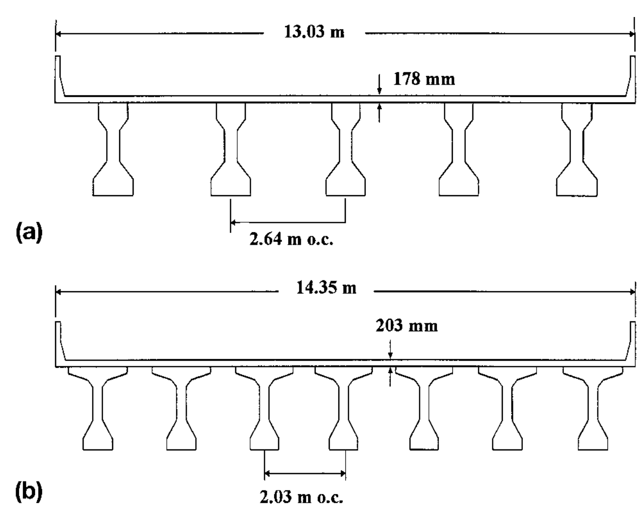

FIG. 5. Cross Sections of Selected Bridges: (a) U.S. 27 Bridge, Fanning Springs, Fla.; (b) I-75 Bridge, Broward County, Fla.

Individual bridge beams from the selected bridges were modeled herein. The analysis of the bearing restraint effects did not incorporate dead loads or prestressing forces in the beams. The study analyzed the relative performance of the beams under live load assuming an initial unloaded condition with the beams at zero initial deflection. Other possible conditions involving thermal change, shrinkage, creep, dynamic effects, and longitudinal load effects were not considered. The entire U.S. 27 bridge segment [Fig. 5(a)] with Type III beams was also modeled. The FE results were compared with results from FDOT field tests on the bridge (Issa 1992).

The slab and beam concrete was modeled using the element SOLID65 from ANSYS, which is a 3D element with eight nodes. Each node has three translational degrees of freedom. The element is nonlinear and has the capability of cracking in tension and crushing in compression in addition to plasticity and creep. The behavior of the bridges under service loads fell well within the elastic region and SOLID65 was used as a linear element by removing the cracking and crushing properties. Smeared reinforcements were used to simulate the reinforcement in the beam and slab models.

The bearing pads were remodeled with a series of spring elements, COMBIN14 from ANSYS. The pad models were changed to reduce the number of elements and run time. The elements were arrayed horizontally and vertically to simulate the shear and compression load/displacement characteristics of the bearing pads. The models were also analyzed with the conventional simple hinge/roller support condition, in order to measure the relative effect of increasing bearing stiffness.

TABLE 4. FE Model Parameters

Model data (1)	AASHTO Type III beam (2)	AASHTO Type V beam (3)	U.S. 27 full bridge (4)
Nodes	14,456	7,676	10,079
Total elements	13,072	5,616	6,856
SOLID65	12,064	5,576	6,656
COMBIN14	144	40	200
Concrete Poisson's ratio	0.18	0.18	0.18
Beam E (MPa)	2.78×10^4	3.21×10^4	2.78×10^4
Slab E (MPa)	2.23×10^4	2.51×10^4	2.23×10^4
Steel Poisson's ratio	0.29	0.29	0.29
Flexural reinforcement E (MPa)	1.90×10^5	1.90×10^5	1.90×10^5
Slab rebars E (MPa)	2.00×10^5	2.0×10^5	2.00×10^5

INDIVIDUAL BEAM AND BEARING PAD MODELS

The ANSYS FE model parameters for AASHTO Types III and V beams are presented in Table 4. The total number of elements used was decreased for the AASHTO Type V beam model to decrease computer run time, which did not significantly affect the accuracy of the results. A full AASHTO HS20-44 truckloading, together with AASHTO impact factors, was distributed at three nodes along the length of each beam to produce maximum bending moments.

The difference between the bottom flange width and bearing pad width was about 100 mm for both beams. This small difference was neglected for simplicity, and the spring elements were distributed over a bearing surface corresponding to the flange width and the pad length. Nodes on the beams were connected by the spring elements to matching fixed node sets located below and to the sides of the beams for the vertical and horizontal spring elements, respectively.

Individual spring stiffness values were based on the appropriate tributary area. The sum of the individual spring constants equaled the pad stiffness values presented in Figs. 3 and 4. The vertical springs were categorized as corner, edge, and center, depending on the location within the bearing surface. The horizontal elements were arrayed in single lines parallel to the bottom flange of the beam. Table 5 presents the element and stiffness details. The torsional stiffnesses and bending stiffnesses were indirectly accounted for due to the symmetric placement of the vertical springs about the y- and z-axes of the bearing pad model (Fig. 2).

Average FE beam nodal results were compared for the simple supports and the spring supports with increasing stiffnesses. Maximum vertical deflections, compressive stresses, tensile stresses, longitudinal end movement, and horizontal restraining forces at beam ends are presented in Table 6. A zero shear modulus represents simple support conditions in this table. The percent change in various parameters as compared to the values for simple support conditions are presented in Table 7.

The restraint effects of the bearing pads were found to be beneficial to the performance of the beams. The bearing pads

TABLE 5. Spring Stiffness Values for FE Beam Models

Type of element (1)	Number of elements (2)	Fraction of total stiffness (3)	Spring Stiffness (kN/mm) G = 0.655 MPa (4)	G = 0.896 MPa (5)	G = 1.379 MPa (6)
(a) AASHTO Type III (Horizontal), k_z					
Total horizontal elements	12	Full	1.93	2.63	4.05
Outer springs	2	1/22	0.09	0.12	0.18
Inner springs	10	1/11	0.18	0.24	0.37
(b) AASHTO Type III (Vertical), k_x					
Total vertical elements	60	Full	736	1,016	1,576
Corner springs	4	1/176	4.18	5.77	8.96
Edge springs	26	1/88	8.36	11.54	17.91
Center springs	30	1/44	16.7	23.08	35.82
(c) AASHTO Type V (Horizontal), k_z					
Total horizontal elements					
Outer springs	5	Full	2.61	3.57	5.48
Inner springs	2	1/8	0.33	0.45	0.69
	3	1/4	0.65	0.89	1.37
(d) AASHTO Type V (Vertical), k_x					
Total vertical elements	15	Full	995	1,363	2,102
Corner springs	4	1/32	32	43	66
Edge springs	8	1/16	62	85	131
Center springs	3	1/8	124	170	263

TABLE 6. Variations in Performance Parameters of AASHTO Beams

Shear modulus of bearing pad (MPa) (1)	Maximum midspan deflection (mm) (2)	Maximum compressive stress (MPa) (3)	Maximum tensile stress (MPa) (4)	Longitudinal end movement (mm) (5)	Horizontal restraint force (kN) (6)
(a) AASHTO Type III Beam					
0	15.01	9.04	4.75	1.94	0
0.655	14.76	8.57	4.69	1.83	3.53
0.896	14.63	8.56	4.68	1.83	4.80
1.379	14.48	8.52	4.67	1.80	7.32
(b) AASHTO Type V Beam					
0	38.00	5.64	9.51	3.89	0
0.655	36.93	5.56	9.34	3.15	8.20
0.896	36.70	5.54	9.31	3.12	11.13
1.379	36.35	5.51	9.25	3.10	16.59

TABLE 7. Percent Change in Parameters for AASHTO Beams, in Relation to Simple Support Conditions

Shear modulus of bearing pad (MPa) (1)	Maximum vertical deflection (%) (2)	Maximum compressive stress (%) (3)	Maximum tensile stress (%) (4)	Longitudinal beam end movement (%) (5)
(a) AASHTO Type III Beam				
0.655	−1.7	−1.3	−5.2	−5.9
0.896	−2.5	−1.4	−5.3	−5.9
1.379	−3.6	−1.8	−5.7	−7.2
(b) AASHTO Type V Beam				
0.655	−2.8	−1.5	−1.7	−19.0
0.896	−3.4	−1.7	−2.1	−19.6
1.379	−4.3	−2.2	−2.8	−20.3

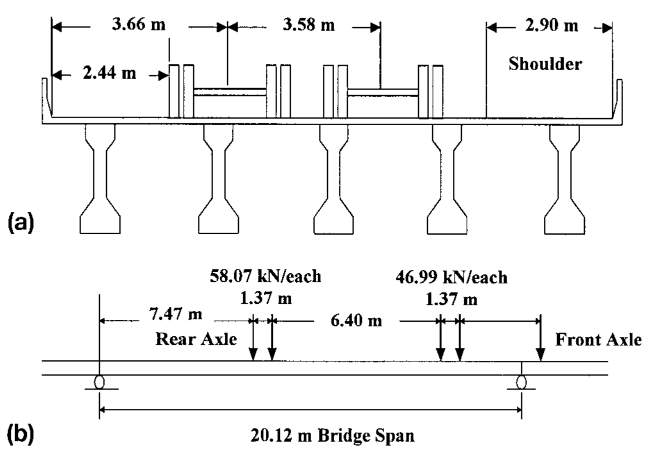

FIG. 6. Load Positions on U.S. 27 Bridge, FDOT Field Test: (a) Lateral; (b) Longitudinal

resist the outward movement of the lower flanges at the beam ends. The restraint forces acting inward at the bottom of the flange produce a negative moment that counteracts the positive live load moment. It was observed that the largest beneficial effects were realized with the highest elastomer shear modulus.

The restraint effects for the Type III beam produced small reductions in deflection and compressive stress. Somewhat larger effects were realized for tensile stresses, with reductions of >5%, compared to simple support conditions. However, the effect of end restraints on the displacement and stresses were found to be small, even for an increased shear modulus of 1.379 MPa. The largest effect was in reducing the horizontal displacement by nearly 20% in the Type V beam.

U.S. 27 FULL BRIDGE MODEL

The number of elements was reduced in each beam for the U.S. 27 bridge model in order to conform to ANSYS limitations. During the FDOT field test, two tractor trailers weighing 914 kN each were placed on the bridge to cause maximum applied moment (Issa 1992). The front wheels were located off span, and the centers of the tractor and trailer tandems were positioned at 8.15 and 15.95 m, respectively, from the other end of the span [Fig. 6(b)]. The trucks were located side by side on the bridge, with the first and the second trucks at 3.66 and 7.24 m, respectively, from the inside face of the barrier [Fig. 6(a)].

The parameters presented in Table 4 were used in the ANSYS FE model of the bridge segment. The vertical and horizontal bearing spring details are presented in Table 8. To account for the increase in bearing stiffness due to age or cold temperatures, additional elastomer shear modulus values of 6.89 and 34.47 MPa (corresponding to 1,000 and 5,000 psi) were used in the full bridge analysis.

Average maximum nodal deflections and tensile strains obtained at the bottom of each beam flange at midspan from the FE analysis are presented in Figs. 7 and 8, respectively. These

TABLE 8. U.S. 27 Full Bridge Spring Stiffness Values

Type of element (1)	Number of elements (2)	Fraction of total stiffness (3)	Spring Stiffness (kN/mm)		
			G = 0.655 MPa (4)	G = 0.896 MPa (5)	G = 1.379 MPa (6)
(a) AASHTO Type III (Horizontal), k_z					
Horizontal elements	5	Full	1.93	2.63	4.05
Outer springs	2	1/8	0.24	0.33	0.51
Inner springs	3	1/4	0.48	0.66	1.01
(b) AASHTO Type III (Vertical), k_x					
Vertical elements	15	Full	736	1,016	1,576
Corner springs	4	1/32	23	32	44
Edge springs	8	1/16	46	63	98
Center springs	3	1/8	92	127	197

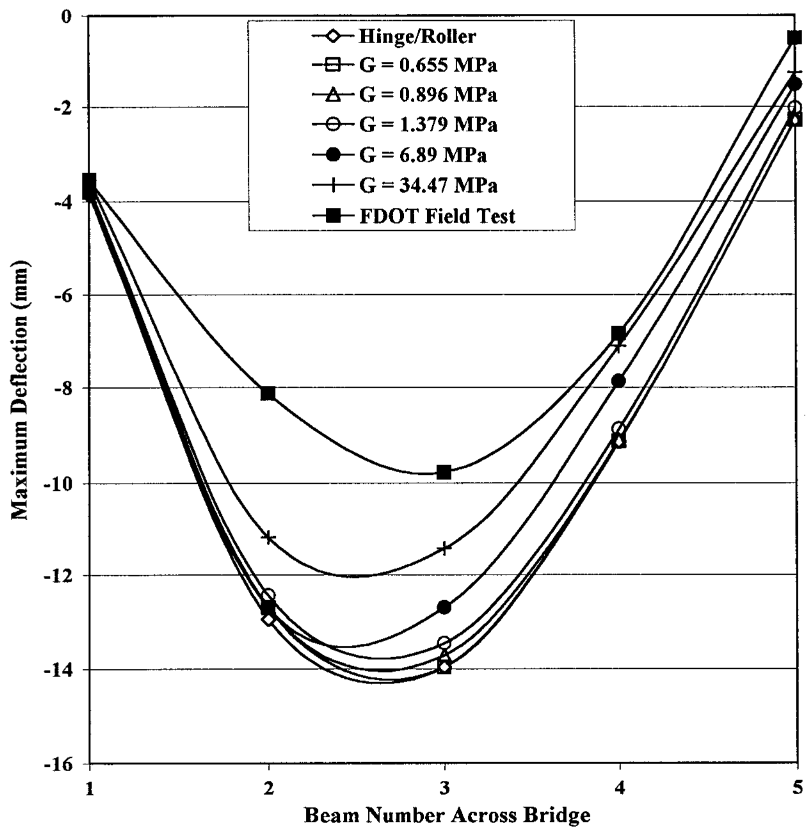

FIG. 7. Maximum Deflections in U.S. 27 Bridge

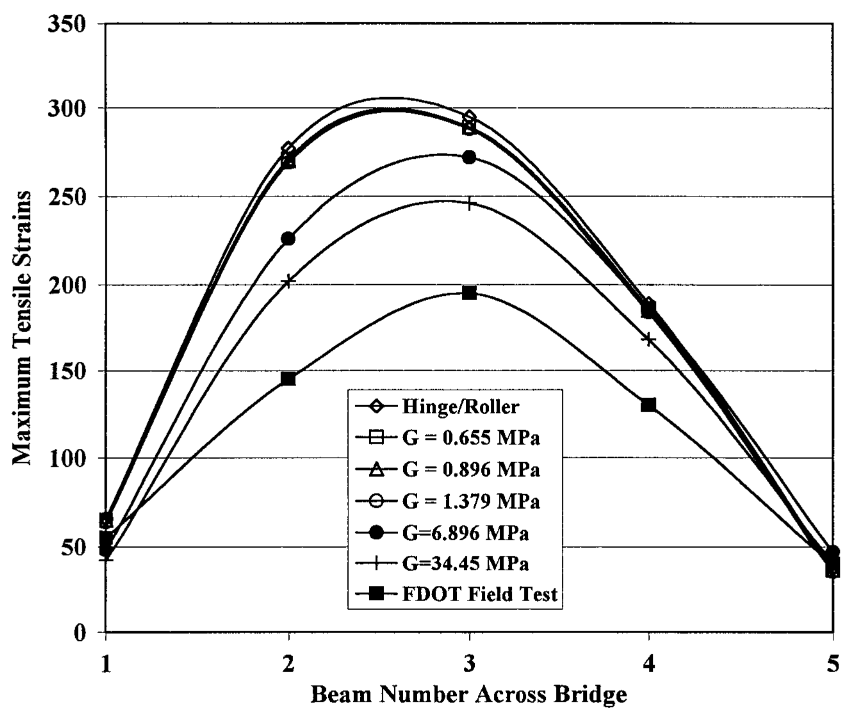

FIG. 8. Maximum Tensile Strains in U.S. 27 Bridge

figures also show the FDOT field test results. The bearing pad effects on the U.S. 27 bridge model were small for normal AASHTO range of shear modulus values from 0.655 to 1.379 MPa. However, for increased shear modulus values, the maximum deflection and tensile strains were appreciably reduced. For increased shear moduli of 6.89 and 34.47 MPa, the deflections were reduced by about 14–28%, respectively, and the maximum tensile strains in the bottom of the critical beam were reduced by 15 and 34%, respectively. In all cases, the bridge FE model predicted greater deflections and strains as compared to the FDOT field test results. It is possible that differences in the constructed bridge from blueprint specifications, such as increased slab thickness at some locations or greater concrete strength, may have resulted

TABLE 9. Variation of Horizontal Restraint with Elastomer Shear Modulus, U.S. 27 Bridge Model

Shear modulus (MPa) (1)	Horizontal Restraint Details: Total restraint for all beams (kN) (2)	Percentage of live load (3)
0.655	9.38	0.5
0.896	12.72	0.7
1.379	19.4	1.06
6.89	89.42	4.89
34.47	355.85	19.47

in a bridge stronger in service than the analytical results suggest.

The details of horizontal restraint forces for all beams in the U.S. 27 bridge model are presented in Table 9. It can be observed that the total horizontal restraint increases gradually for lower shear modulus values (for normal bearing pads) but increases drastically for higher shear moduli (for old bearing pads or colder climates). AASHTO standard specifications (AASHTO 1996a) require that the horizontal forces imparted by the superstructure to the substructure be limited to 5%. The restraint forces are less than this value even for an increased shear modulus of 6.89 MPa. It should be noted that the AASHTO limit may include the breaking forces, which were not considered in this study.

Factors other than those considered in this study may influence the effect of bearing pads on bridge beams. One such factor is the angle of a skewed bridge. The loading angle on the bearing pad and resulting loaded beam bearing surface will change with changes in the skew angle. Current FDOT specifications call for alignment of the pads relative to the support or abutment, not the beams. The effect of other factors such as beam spacing, beam length, temperature, diaphragm action, dynamic response, etc., on the performance of bridges with bearing pads needs to be explored. The use of the FE analysis approach may provide relatively inexpensive answers to questions regarding these effects.

It is difficult to actually quantify the increased stiffness associated with aging elastomeric pads without load tests. If a simple empirical method could be developed to predict the increased stiffness, it could be conveniently applied for evaluation of old bridges. Additional research is needed to develop such empirical methods through the testing of old bearing pads.

In certain situations, the resistance from the bearing pads may be reversed to a positive bending moment being superimposed on the regular dead and live load moments. This condition may arise at a time of maximum temperature when the beams were set on the pads at extreme cold temperatures and the beams have undergone creep and shrinkage. The horizontal resistance from the bearing pad could be directed outward under these circumstances, increasing the beam positive moment. A follow-up study is being performed at the Florida A. & M. University—Florida State University College of Engineering, in which the bearing pad effect is being expanded to include temperature and diaphragm effects. The reverse condition will be investigated in the follow-up study.

Only expansion type bearings were investigated herein. Fixed-type bearings, which may provide greater horizontal resistance to I-beams, were not considered.

CONCLUSIONS AND RECOMMENDATIONS

The following conclusions may be based upon the findings of this study:

1. The AASHTO specifications provide relatively accurate and convenient methods for predicting the various stiffnesses for elastomeric bridge bearing pads.
2. The performance characteristics of AASHTO precast bridge I-beams are slightly enhanced by the effect of restraints from laminated neoprene bearing pads. The beneficial effects increase with increased stiffness of the bearing pads for the normal range of bearing stiffness specified by AASHTO. In general, the beneficial effect is not significant.
3. The beneficial effects of bearing pads on precast bridge I-beams become more pronounced with a drastic increase of bearing stiffness due to aging and cold temperatures. For a drastic 50 times shear modulus increase up to 34.47 MPa, the beneficial effects on deflection and strain may be in the 28–34% range. Unless such extreme hardening of the bearing pads are encountered, the beneficial effects on bridge beams are minimal. Although a 50 times shear modulus increase is theoretically possible, the actual increase for a particular bridge needs to be justified if the beneficial effects are to be utilized.
4. Ignoring the effects of laminated neoprene bearing pads in the design of AASHTO precast beams subjected to vertical live loads results in a conservative design. Negligence of such effects will result in a nonconservative design for the substructure. However, under certain combinations of temperature and creep/shrinkage effects, the horizontal bearing restraint may be reversed. Ignoring such effects may lead to the nonconservative design for bridge beams. Further investigation in this area is needed.
5. Current FDOT elastomeric expansion bridge bearings are serving the main purpose of their usage, which is to provide minimum horizontal resistance to the beam while allowing horizontal movement.
6. Actual constructed bridges may be stiffer in practice than theoretical analysis would suggest. The difference may be attributed to differences in the constructed bridges from the blueprints such as an increase in slab thickness at certain parts of the bridge, or higher than specified concrete strength.
7. The horizontal restraint forces transferred by the bearing pads to the substructure for the U.S. 27 bridge are small in general, and within AASHTO limits.
8. For significant restraining effects from the bearing pads to be beneficially effective on the beams, more rigid restraining systems and/or interaction between beam ends and abutment walls should be present.

Based on this study, it is recommended that the effects of horizontal bearing restraint be ignored in the design of AASHTO precast concrete bridge I-beams. This effect may be included in the rating of existing bridges, if the increased stiffness of the bearing is justified. Periodic inspection of the bearing pads in service will reveal age-related defects in the neoprene such as cracking or splitting. It is most probable that this condition will be recognized, and the pads will be replaced prior to the substantial shear modulus increase due to age effects. Monitoring of each bridge bearing pad on a periodic basis may be an arduous task. Other more rigid restraining systems and/or interaction between beam ends and abutment walls may be explored if beneficial restraining forces are needed for precast bridge beams.

IMPACT ON BRIDGE ENGINEERING PRACTICE

The findings of the reported study will be beneficial to bridge engineers in understanding the true role of elastomeric bearing pads in the behavior and effect of AASHTO bridge beams and corresponding substructures. For relatively new bearing pads with usual stiffness and thermal conditions, bridge engineers may ignore the small friction forces imparted by the bearing pads on AASHTO beams and substructures. The restraining effects, if considered, will be beneficial in stiffening the beams and decreasing the live load stresses and deflections. Bridge engineers should know that the restraining effects increase significantly if bearing pads stiffen drastically with age, weathering, and cold temperatures. If such beneficial effects are to be considered in bridge design, it must be ensured that the drastic increase in pad stiffening assumed in the design practice is really achieved in practice. Ongoing regular monitoring of bearing pads will be a time-consuming and expensive task.

APPENDIX I. REFERENCES

AASHTO. (1996a). *AASHTO LRFD bridge design specifications*, Washington, D.C.

AASHTO. (1996b). *Standard specifications for highway bridges*, 16th Ed., Washington, D.C.

ANSYS structural nonlinearities: User's guide for revision 5.1. (1995). Vol. I and II, SAS IP.

Bakht, B. (1988a). ''Observed behaviour of a new medium span slab-on-beam bridge.'' *Struct. Res. Rep. SRR-88-01*, Ministry of Transportation, Ontario, Canada.

Bakht, B. (1988b). ''Testing of an old short span slab-on-beam bridge.'' *Struct. Res. Rep. SRR-88-02*, Ministry of Transportation, Ontario, Canada.

Bakht, B., and Jaeger, L. G. (1988). ''Bearing restraint in slab-on-girder bridges.'' *J. Struct. Engrg.*, ASCE, 114(12), 2724–2740.

Bakht, B., and Jaeger, L. G. (1992). ''Ultimate load test of slab-on-girder bridge.'' *J. Struct. Engrg.*, ASCE, 118(6), 1608–1624.

Billing, J. R. (1984). ''Dynamic loading and testing of bridges in Ontario.'' *Can. J. Civ. Engrg.*, Ottawa, 11, 823–843.

''Standard drawings.'' (1996). *Struct. Des. Ofc.*, Florida Department of Transportation, Tallahassee, Fla.

''Structures design guidelines.'' (1997). *Struct. Des. Ofc.*, Florida Department of Transportation, Tallahassee, Fla.

Issa, M. (1992). ''Dynamic and static tests of prestressed concrete beam bridges in Florida.'' *Struct. Res. Ctr., MS 80*, Florida Department of Transportation, Tallahassee, Fla.

Minor, J., and Egen, R. (1970). ''Elastomeric bearing research.'' *Nat. Cooperative Hwy. Res. Program Rep. 109*, Transportation Research Board, Washington, D.C.

Pentas, H. A., Avent, R. R., Gopu, V. K., and Rabello, K. J. (1995). ''Field study of longitudinal movements in composite bridges.'' *Transp. Res. Rec. 1476*, Transportation Research Board, Washington, D.C., 117–128.

Ramachandran, U. (1994). ''Restraint effect of bearings.'' MSCE thesis, University of South Florida, Tampa, Fla.

Roeder, C. W., Stanton, J. F., and Taylor, A. W. (1987). ''Performance of elastomeric bearings.'' *Nat. Cooperative Hwy. Res. Program Rep. 298*, Transportation Research Board, Washington, D.C.

Roeder, C. W., Stanton, J. F., and Feller, T. (1989). ''Low temperature behavior and acceptance criteria for elastomeric bridge bearings.'' *Nat. Cooperative Hwy. Res. Program Rep. 325*, Transportation Research Board, Washington, D.C.

Sen, R., and Spillet, K. (1994). ''Restraint effects of bearings (Phase I).'' *Final Rep. Catalog No. 2104-168-LO*, Florida Department of Transportation, Tallahassee, Fla.

APPENDIX II. NOTATION

The following symbols are used in this paper:

A_x, A_y, A_z = cross-sectional areas corresponding to each axis;
E = modulus of elasticity;
E_c = effective compressive modulus;
G = shear modulus of elasticity;
H = total thickness of bearing excluding rigid plates;
h_{ri} = thickness of single elastomer layer;
I_x, I_y, I_z = moments of inertia corresponding to each axis;
k = empirical constant dependent on elastomer hardness;
k_{Rx}, k_{Ry}, k_{Rz} = equivalent stiffness corresponding to Δ_{Rx}, Δ_{Ry}, Δ_{Rz}, respectively;
k_x, k_y, k_z = equivalent stiffness corresponding to Δ_x, Δ_y, Δ_z, respectively;
L = dimension of bearing parallel to longitudinal beam axis;
M_x, M_y, M_z = moments applied about x-, y-, and z-axes respectively;
P_x, P_y, P_z = forces applied in x-, y-, and z-directions, respectively;
S = shape factor from individual layer of elastomeric bearing;
W = dimension of bearing normal to beam axis;
Δ_{Rx}, Δ_{Ry}, Δ_{Rz} = rotations corresponding to M_x, M_y, M_z, respectively; and
Δ_x, Δ_y, Δ_z = deflections corresponding to P_x, P_y, P_z, respectively.